P1.1 THE DEVELOPMENT OF THE HOWARD UNIVERSITY RAMAN LIDAR

Demetrius Venable[1,*], Everette Joseph[1], David Whiteman[2], Belay Demoz[2],
Rasheen Connell[1], and Segayle Walford[1]
[1]*Howard University, Washington, DC 20059*
[2]*NASA Goddard Space Flight Center, Greenbelt, MD 20771*

1. INTRODUCTION

We have established a collaborative effort to develop a Raman lidar system that is designed to make both daytime and nighttime measurements of atmospheric water vapor and aerosols. The three-channel lidar system's laser operates at the third harmonic of Nd:YAG. The lidar uses narrow bandpass filters to measure (1) the elastic back-scattered and pure rotational Raman signals at 354.7 nm, (2) the Raman scattered photons from nitrogen molecules at 386.7 nm, and (3) the Raman scattered photons from water vapor molecules at 407.5 nm. One of the primary purposes of the lidar is to characterize the temporal and vertical distributions of water vapor and dynamics processes in the boundary layer for evaluation of mesoscale models. The lidar is also used to measure cirrus cloud optical depths. The collaboration consists of researchers from the Department of Physics and the Program in Atmospheric Sciences at Howard University and the Laboratory for Atmospheres at the NASA Goddard Space Flight Center. These collaborators have designed, constructed, and performed initial testing of the Howard University Raman Lidar (HURL) System.

2. DESCRIPTION OF THE LIDAR SYSTEM

HURL was initially designed to measure water vapor and aerosols under the following assumptions:

- daytime measurements comparable to the CART [Goldsmith 1998] Raman Lidar;
- initial configuration allowing water vapor mixing ratio and aerosol scattering ratio measurements;
- no aerosol extinction measurements below ~3km in altitude using a vertical pointing configuration (i.e. good for cirrus optical depth but not for boundary layer aerosol optical depth);
- three-channel system; and
- photon counting detector system.

The basic components of the system are shown in the Block Diagram in Figure 1. The laser is a Continuum Lasers Precision II 9030. This is a Nd:YAG laser which provides an average output power of 48 W at the fundamental wavelength and is capable of lasing at the second, third, and fourth harmonics. The system utilizes a configuration that consists of an oscillator and two amplifiers and operates at a rep-rate of 30 Hz. Our system is designed to operated at the third harmonic (354.7 nm) and provides a maximum average power of 14 W at this wavelength. Our typical operating average power is about 10 W. The beam divergence is 0.5 mrad and the beam profile is nearly Gaussian in the far field (correlation coefficient of 0.9 when compared to a Gaussian profile using least squares analysis.) The beam diameter is 9.5 mm at the laser exit. Cooling of the laser is provided with a closed-loop 4 kW air-cooled Affinity chiller.

Techniques have been employed to make the entire system eye safe to aircraft flying over the site. This is accomplished by expanding the laser beam with a 15X Beam Expander before exiting the laboratory. The beam expander consists of a 25.4 mm diameter, 500 mm focal length entrance lens and two 150 mm diameter exit lenses, each with 1000 mm focal length. The lenses are placed in a rigid metering rod assembly and enclosed in an isolated metal assembly. Light exiting the beam expander is incident on a transmitter mirror that is used to align the beam with the telescope's field of view. The transmitter mirror is mounted in a modified Newport Corporation SL-A Series gimble mount that is driven by Newport Ultra-resolution electrostrictive actuators providing 0.04 μm minimum incremental motion. This provides an angular resolution of better than 1 μrad. The optics are optimized for transmission of the 354.7 nm laser light.

The bi-axial system (separation between the outgoing laser beam and telescope central axis is

*Corresponding author address: Demetrius Venable, Department of Physics and Astronomy, Howard University, 2355 6th St., NW, Washington, DC 20059; email: dvenable@howard.edu.

less than 45 cm) utilizes a 400 mm aperture f/2.3 (focal length of 921 mm) fiber coupled coaxial telescope. The primary and secondary reflectors use UV enhanced aluminum optical coating that provides a reflectivity greater than 92% at 355 nm. The telescope field of view is 250 μrad with a 365 μm diameter fiber located at the field stop. The entire optical system, including the telescope, is designed to be stable for a temperature change of ±15 °C. The combination of system alignment, telescope field-of-view, and laser beam divergence allows for full overlap of the laser beam within the telescope field-of-view at altitudes above 3.5 km. This gives the system an effective operating range of ~1 km to ~15 km. The telescope and beam expander were designed and built by Welch Mechanical Designs.

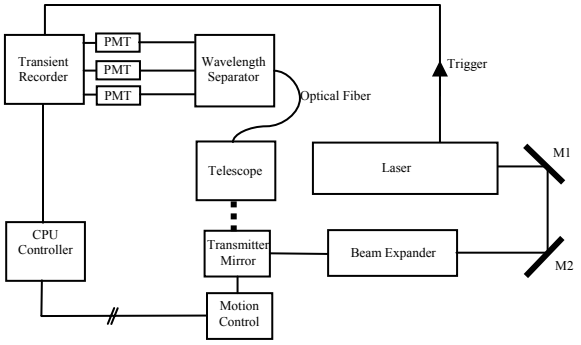

Figure 1. Block Diagram of the HURL Raman Lidar. The components of the system are described in detail in the text of this paper.

Wavelength separation of the returned signal is accomplished using a wavelength separation system also designed and manufactured by Welch Mechanical Designs. The system accepts a fiber optic from the telescope and collimates the light from this fiber using two Melles Griot fused quartz lenses with an overall effective focal length of 75 mm. This light is split into three "channels" by the use of two beam splitters manufactured by Barr Associates. The first beam splitter is designed to reflect all light below 360 nm (specifically the 354.7 nm component) and transmit all higher wavelengths. The transmitted light is further separated by a second beam splitter that reflects all light above 400 nm (specifically the 408.7 nm component) and transmits light at lower wavelengths (specifically the 387.5 nm component). Each of these three components of the light is transmitted to an appropriate wavelength channel that contains optical components to further isolate the desired wavelength and image the light onto a photomultiplier tube. Each channel contains a narrow bandpass filter for the appropriate wavelength also manufactured by Barr Associates. The band widths are approximately 0.25 nm in each case and the transmission of the filters ranges from 30 to 45%. The photomultiplier tubes used are the Hamamatsu Corporation Model R1924P. These tubes provide high radiant sensitivity and low dark current.

The Data Acquisition System consists of Optical Transient Recorders manufactured by Licel Corporation that are capable of simultaneous analog and photon counting acquisition. Since nonlinearities in photon counting rates can become significant at counts rates on the order of 10 MHz, the combined analog-photon counting detection can increase the dynamic range significantly, up to virtual count rates of 1 GHz. A 12 bit – 40 MHz A/D converter is used to digitize the analog signal. Photon counting uses a fast three-stage preamplifier and a discriminator with 64 threshold levels and operates at 250 MHz. The entire system is controlled with a LabView interface via a PCI-DIO32HS card. The CPU operates with a 3.06 GHz processor, has 3.00 GB of RAM, and a 112 GB hard disk. Figure 2 shows a view of the user interface window running under LabView.

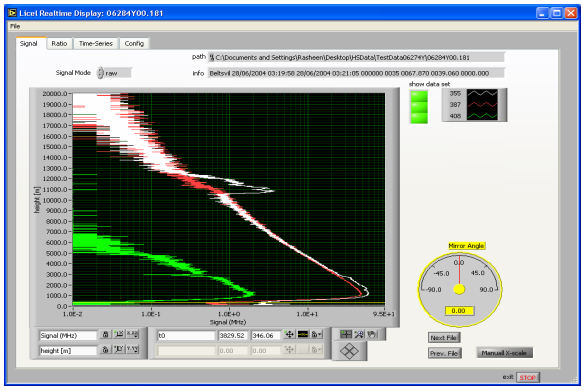

Figure 2. LabView user interface window for real time display of acquired data.

3. ANALYSIS OF INITIAL LIDAR DATA

When processing raw data, a variety of corrections should be applied to obtain the best results. These include resolving time correction, correction for dark-current, background subtraction, range square correction, overlap function correction, noise reduction correction, correction for differential absorption and correction for temperature effects. Data smoothing includes techniques such

as merging and smoothing of bins over altitude and combining of profiles over time. These smoothing techniques may range from simple averaging to Fast Fourier Transforms.

The backscattered signal includes primarily the Rayleigh and Mie scattering components from air molecules and aerosols. In the single scattering regime, the power received as a function of range, z, after subtraction of any background component, is given by S_R where, [Whiteman 2003]

$$S_R(\lambda_L,z)=\frac{\left\{N_R(z)d\sigma_R(\lambda_L,\pi)/d\Omega+\beta_\pi^{aer}(\lambda_L,z)\right\}}{z^2}O_L(z)\times I_L(\lambda_L)A\varepsilon(\lambda_L)\exp\left[-2\int_0^z\alpha(\lambda_L,z')dz'\right]. \quad (1)$$

λ_L *is* the wavelength of the laser photons, $O_L(z)$ is defined to be the overlap function for the channel corresponding to wavelength λ_L, $I_L(\lambda_L)$ is output power of the laser, A is the area of the telescope, $\varepsilon(\lambda_L)$ is the efficiency of the system for photons of wavelength λ_L, $N_R(z)$ is the concentration density of air molecules, $d\sigma_R(\lambda_L, \pi)/d\Omega$ is the Rayleigh backscatter cross section, and $\beta_\pi^{aer}(\lambda_L, \pi)$ is the aerosol backscatter cross section. Finally $\alpha(\lambda_L, z)$ is the total extension coefficient of the laser photons along the path of the beam.

The power received at the detector at the wavelengths corresponding to the Raman scattered signals as a function of range, after subtraction of any background component, is given by S_X, where [Whiteman 2003]

$$S_X(\lambda_X,z)=\frac{N_X(z)\left\{d\sigma_X(\lambda_L,\pi)/d\Omega\right\}}{z^2}O_X(z)I_L(\lambda_L)A\varepsilon(\lambda_X)\times\exp\left[-\int_0^z\left[\alpha(\lambda_L,z')+\alpha(\lambda_X,z')\right]dz'\right]. \quad (2)$$

The various terms are defined as above with the subscript X representing the molecular scattering species (X→N for nitrogen and X→H for water vapor) considered in our analysis. This equation differs from Eq. 1 in that the aerosol backscatter contribution is omitted, there is a wavelength transition from λ_L to λ_X corresponding to the Raman wavelength shift that occurs for the inelastic scattering event, and the exponential term includes an attenuation factor for the outgoing laser beam at λ_L and the returning beam at λ_X. For these equations we have not yet considered any contribution due to temperature effects which are discussed below.

The signal that is referred to as the Rayleigh/Mie component in this paper actually contains both the elastically scattered signal at the laser wavelength and the pure rotational Raman signal centered at the laser wavelength (primarily due to scattering from N_2 and O_2). This rotational Raman signal is temperature dependent. If the bandpass filters that are used in the system are sufficiently narrow so that all of the rotational components are not encompassed by the filter, the temperature dependence of the signal must be taken in consideration. This is the case for our system ($\Delta\lambda_L$ ~ 0.25 nm for our filters). This is also true for the rotational states centered at the vibrational transition wavelengths for water vapor and nitrogen. Whiteman has show that the temperature dependence can be accounted for by [Whiteman 2003]

$$d\sigma_X(\lambda_L,\pi,T)/d\Omega\rightarrow F_X(T)\left[d\sigma_X(\pi)/d\Omega\right] \quad (3a)$$

$$d\sigma_R(\lambda_L,\pi,T)/d\Omega\rightarrow F_R(T)\left[d\sigma_R(\pi)/d\Omega\right]. \quad (3b)$$

F(T) is a term that accounts all for the temperature dependence in the lidar equation.

The water vapor mixing ratio is defined as the mass of the water vapor in a given volume divided by the mass of the dry air in that volume. Since nitrogen is assumed to be in constant proportion to the amount of dry air, we use the amount of nitrogen as a measure of dry air when determining the water vapor mixing ratio. Then, using Eqs. 1, 2, and 3 one obtains an operational equation for the water vapor mixing ratio, *w*, where

$$w(z)=\frac{N_H(z)M_H}{N_{dryair}(z)M_{dryair}}=f\exp\left[-\int_0^z\left[\alpha(\lambda_N,z')+\alpha(\lambda_H,z')\right]dz'\right] \quad (4a)$$

and

$$f=\frac{S_H(\lambda_H,z)}{S_N(\lambda_N,z)}\frac{M_H}{M_{dryair}/0.78}\times\frac{O_N(z)\varepsilon(\lambda_N)F_N(T)\left\{d\sigma_N(\lambda_L,\pi)/d\Omega\right\}}{O_H(z)\varepsilon(\lambda_H)F_H(T)\left\{d\sigma_H(\lambda_L,\pi)/d\Omega\right\}} \quad (4b)$$

is the system calibration constant for the water vapor mixing ratio. M_H is the molecular weight of water vapor and M_{dryair} is the molecular weight of nitrogen. Here we have taken into account the

relative amount of N_2 in a given volume of dry air and used the N_2 lidar signal, S_N, as a measure of the amount of dry air.

The aerosol scattering ratio can be determined from the ratio of $S_R(\lambda_L, z)$ and $S_N(\lambda_L, z)$, i.e.

$$\frac{S_R(\lambda_R,z)}{S_N(\lambda_N,z)} = \frac{O_R(z)\varepsilon(\lambda_L)\left\{F_R(T)\beta_\pi^{mol}(\lambda_L,z)+\beta_\pi^{aer}(\lambda_L,z)\right\}}{O_N(z)\varepsilon(\lambda_N)F_N(T)\beta_\pi^{N}(\lambda_L,z)} \times \exp\left[-\int_0^z\left[\alpha(\lambda_N,z')+\alpha(\lambda_L,z')\right]dz'\right], \quad (5)$$

where

$\beta_\pi^{mol}(\lambda_L,z) = N_R(z)\,d\sigma_R(\lambda_L,\pi)/d\Omega$, and

$\beta_\pi^{N}(\lambda_L,z) = N_N(z)\,d\sigma_N(\lambda_L,\pi)/d\Omega$.

Since N_2 is well mixed in the region of the atmosphere with which we are concerned, the Raman backscatter coefficient β_π^N can be assumed to be proportional to the Rayleigh backscatter coefficient β_π^{mol}, i.e.,

$$\beta_\pi^N(\lambda_L,z) = \frac{1}{k'}\beta_\pi^{mol}(\lambda_L,z)$$

for constant k', then,

$$\frac{S_R(\lambda_R,z)}{S_N(\lambda_N,z)} = \frac{O_R(z)\varepsilon(\lambda_L)}{O_N(z)\varepsilon(\lambda_N)}\frac{F_R(T)\beta_\pi^{mol}(\lambda_L,z)+\beta_\pi^{aer}(\lambda_L,z)}{F_N(T)\beta_\pi^{mol}(\lambda_L,z)} \times k'\exp\left[-\int_0^z\left[\alpha(\lambda_N,z')+\alpha(\lambda_L,z')\right]dz'\right]. \quad (6)$$

Equations 1 - 6 taken from Whiteman [Whiteman 2003] represent the basis for the operation of the Howard University Raman Lidar. The water vapor mixing ration is calculated from Eq. 4 and aerosol back scatter coefficient is determined from Eq. 6 after appropriate normalization. In practice the lidar signal is compared to other instruments for the purpose of calibrating the system. We will accomplish calibration by comparison to radiosondes, a microwave radiometer, and an established Raman Lidar system.

Data were obtained during a twenty-four hour period June 26 - June 27, 2004. Results are shown for a single 1-minute averaged data run in Figure 3. The abscissa gives the counting signal strength in units of MHz. The upper trace is for the Rayleigh-Mie signal at 354.7 nm, the intermediate trace is for the 386.7 nm N_2 Raman signal, and the lower trace is for the 407.5 nm water vapor Raman signal. The 407.5 nm signal has been scaled for display on the graph. These data were taken at approximately 10:30 PM on June 26th. The data are ranged-squared corrected and have special resolution of 75 m. The aerosol data show evidence of low clouds at approximately 3 km and higher altitude clouds at about 12 km.

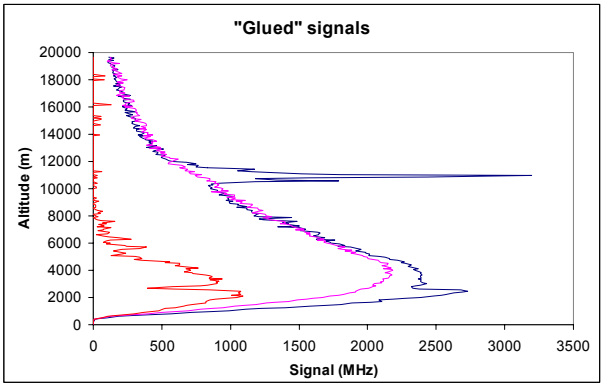

Figure 3. Combined ("glued") ranged-corrected signals from the analog and photon counting detector system. The abscissa gives the counting signal strength in units of MHz. The blue trace is for the 354.7 nm signal, the purple signal is for the 387.5 nm signal, and the red trace is for the 408.7 nm signal. The water vapor data have been scaled to fit on the graph. The spatial resolution for these data is 75 m.

Figure 4 shows the same data with the Rayleigh-Mie signal and the water vapor signal normalized by the nitrogen signal. In these analyses we take advantage of the fact that the quantity of nitrogen is stable in the lower atmosphere.

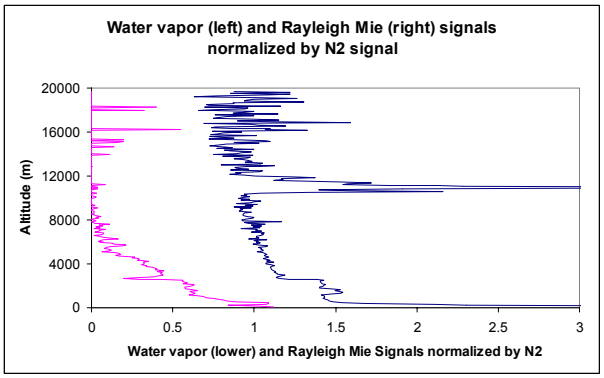

Figure 4. Ratio of the water vapor signal to N_2 signal (purple) and Rayleigh-Mie signal to N_2 signal (blue) for the data shown in Figure 3. The water vapor data have been scaled to fit on the graph.

Time-series plots for data obtained during the full 24-hour period of operation of the lidar are show in Figures 5 and 6. We are currently applying the data corrections and data reduction techniques indicated at the beginning of this section to data we have obtained with our system. We

are in the process of evaluating these techniques to determine how they enhance the signal to noise ratio.

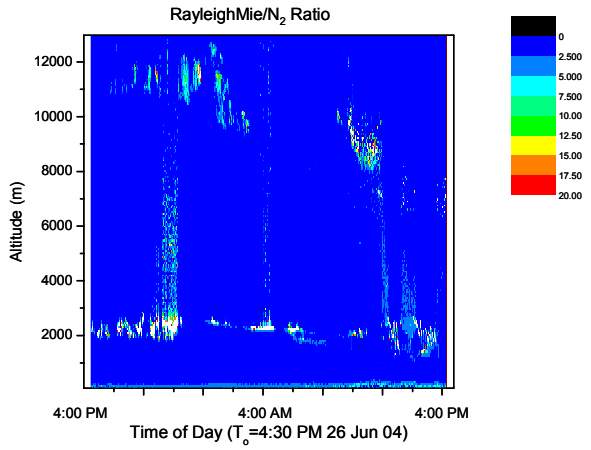

Figure 5. Time-series of data taken June 26 - June 27, 2004 for the aerosol channel normalized by the N_2 channel. Both the low cloud and high cloud features observed in Figure 3 are apparent in this figure. The x-axis is given in units of local Eastern Daylight-Savings Time (EDT).

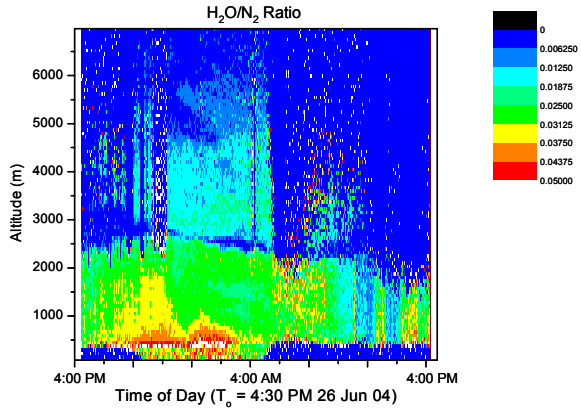

Figure 6. Time-series of data taken June 26 - June 27, 2004 for the water vapor channel normalized by the N_2 channel. Evidence of the boundary layer is apparent near 2700 m. Current efforts are being made to improve the signal to noise ratio. The x-axis is given in units of EDT.

Finally, the water vapor mixing ratio obtained from the lidar data was compared to water vapor mixing ratio calculated from data collected with a radiosonde launch. (The radiosonde system used a Modem SR2K2 403 MHz model by International Met Systems. The sondes were model GL 98.) As a specific example we use the data obtained on June 26, 2004 at 9:00 PM EDT. These results are shown in figure 7. Our results show good qualitative agreement with the radiosonde data. It is expected that these results will improve when additional correction techniques are fully applied to the data. These preliminary data give a system calibration constant for the water vapor mixing ration of 230 ± 20 g/kg. We have not yet taken into account the correction factor for the differential scattering term, the overlap correction, or the temperature dependence in Eq. 4. It is expected that these corrections will result in several percentage points change in the calibration constant. However, the application of the proper corrections for the overlap function should improve the agreement with the lidar and radiosondes data at lower altitudes. Thus, lowering the minimum altitude that usable data can be obtained with the lidar by several hundred meters.

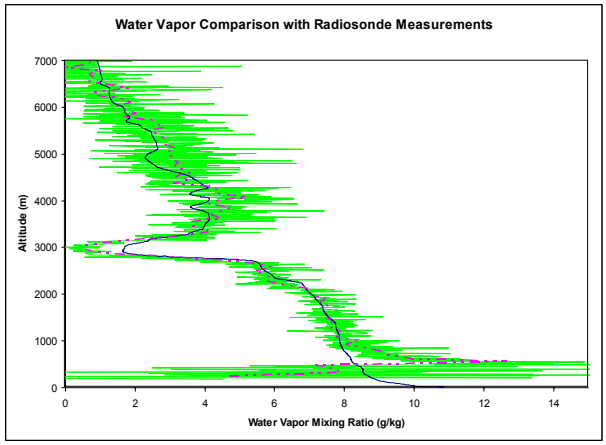

Figure 7. Comparison of the ratio S(408)/S(387) and data obtained from a radiosonde balloon launch (solid black) for June 26, 2004 at 9:00 PM EDT. The green line is for lidar data with 7.5 m resolution and no smoothing techniques applied to the raw data. The dashed line (red) is for the same lidar data but with a spatial resolution of 75 m. (The radiosonde data were supplied by M. Robjhon and S. Walford, Howard University.)

4. SUMMARY

In summary, we have described a collaborative effort to build a three-channel Raman lidar system that is designed to make both daytime and nighttime measurements of water vapor mixing ratios, aerosol backscatter coefficients, and cirrus clouds thicknesses. We have presented results from the first operation of the system and have suggested several techniques that will be used to improve signal to noise ratio as well as several data corrections techniques that will be applied.

Our preliminary results show good qualitative agreement with data obtained from radiosonde measurements for water vapor. The system has met or exceeded all initial design criteria. Preliminary analyses of early data from the system suggest that the lidar is capable of providing the data required for characterization of the temporal and vertical distributions of water vapor and measurement of dynamics processes in the boundary layer; as well as provide adequate data to measure cirrus cloud optical depths.

5. ACKNOWLEDGEMENTS

The authors wish to acknowledge the assistance of Wayne Welch of Welch Mechanical Design for his invaluable help in the design of the system. We also wish to acknowledge Luis Ramos-Izquierdo for his assistance with the optical studies and Fredrick Marsh for his technical assistance. This research has been supported in part by NOAA Grant NA17AE1623, NASA Grant NNG04GD37A, and NSF/HUCOSM Grant 04-003.

6. REFERENCES

Goldsmith, J. E. M, F. H. Blair, S. E. Bisson, and D. D. Turner, Turn-key Raman lidar for profiling atmospheric water vapor, clouds, and aerosols, *Applied Optics*, **37**, 4979-4990, 1998

Whiteman, David, Examination of the traditional Raman lidar technique I, *Applied Optics*, **42**, 2571-2592, 2003

Whiteman, David, Examination of the traditional Raman lidar technique II, *Applied Optics*, **42**, 2593-2608, 2003